Luminescence properties of ZrO_2-CaO eutectic crystals with ordered lamellar microstructure activated with Er^{3+} ions

R. I. Merino, J. A. Pardo, J. I. Peña, G. F. de la Fuente, A. Larrea, and V. M. Orera
Instituto de Ciencia de Materiales de Aragón, Consejo Superior de Investigaciones Científicas-Universidad de Zaragoza, 50009 Zaragoza, Spain
(Received 19 June 1997)

Er^{3+}-doped ZrO_2-CaO eutectic crystals with ordered microstructure have been grown by the laser floating zone method. The microstructure consists of alternating 2 μm thick lamellae of calcia-stabilized zirconia (CaSZ) and $CaZrO_3$ crystals. Er^{3+} enters both phases but at a higher concentration in CaSZ. Due to its higher refractive index, the latter phase acts as a light guiding medium. The optical properties of Er^{3+}-doped eutectic, as well as its components, CaSZ and $CaZrO_3$ crystals, are analyzed. Absorption and emission spectra of $CaZrO_3$ consist of narrow bands. For this crystal most of the Er^{3+} Stark level positions are given. In contrast, the bands for CaSZ are broad, as it corresponds to a defective material. Absorption oscillator strengths, radiative-transition probabilities and emission lifetimes have been measured at different temperatures, between 600 and 4 K. Absorption oscillator strengths are 1.5 times higher for Er^{3+} in $CaZrO_3$ than in CaSZ, while multiphonon deexcitation probabilities are one order of magnitude smaller, with the exception of the lowest energy $^4I_{13/2} \rightarrow {}^4I_{15/2}$ emission, which presents the maximum quantum efficiency in both phases.
[S0163-1829(97)02342-4]

I. INTRODUCTION

There is a growing interest in passive as well as active planar waveguides for the production of components for integrated optoelectronic systems for communications, sensors, display screens, etc. The search for active media for diode laser pumping, suitable for compact integration and with a high optical efficiency is an active field in materials science. Planar waveguides are usually produced by chemical reactions or by deposition onto a substrate. The active ions and the required refractive index profile are introduced into the material using sophisticated methods such as ion implantation,[1] molecular beam epitaxy,[2] or diffusion of dopants (ion exchange).[3,4]

We have recently started with a different approach to produce microstructured optical materials and succeeded in growing eutectic crystals of wide band-gap materials. When these are grown via directional solidification procedures, ordered arrays of hundreds of alternate lamellae (one-dimensional systems) or fibers embedded in a matrix of different composition (two-dimensional systems) can be produced.[5] There is a perfect match between the phases at an atomic scale, as no dislocations or inclusions are detected at the interface, or at most they are restricted to the first atomic layer. Eutectic crystals also show a much higher thermal stability, resistance to thermal shock, and fracture strength than single crystals or glasses.[6]

In the present work we investigate the likelihood to produce an active optical system based on these kinds of materials. Our work focuses on the optical properties of ZrO_2-CaO eutectics doped with Er^{3+} ions. The materials have been grown by the laser floating zone (LFZ) method and are shaped in the form of long cylinders 2 mm in diameter. They consist of regularly aligned lamellae, about 2 μm thick, of calcium-stabilized zirconia (CaSZ) and calcium zirconate ($CaZrO_3$) single crystals.[6] The LFZ growth procedure allows the production of cylinder or fiber shaped crystals of diameters smaller than 2 mm, down to about 200 μm or less, with the possibility of arriving at flexible fiber production. The width of the lamellae can also be controlled since it is dependent on the growth parameters.

CaSZ and $CaZrO_3$ are transparent from 300 nm in the UV range up to about 15 μm in the IR, where first-order phonon absorption appears. The refractive index contrast is small (about 2.5%), but enough to allow guiding of the visible light along the lamellae that grow parallel to the sample axis. In this way we obtain a stack of planar waveguides where rare-earth ions are introduced just by doping the starting materials with the required concentration before crystal growth.

In this study, Er^{3+} has been chosen as the optically active ion. This ion possesses very intense green and red luminescence bands, as well as the maximum quantum efficiency at 1.5 μm ($^4I_{13/2} \rightarrow {}^4I_{15/2}$), inside the window used for optical communications with silica waveguides. Its spectroscopic characterization in yttria-stabilized zirconia crystals has been performed previously.[7] Lasing of the system with relatively low power threshold was also reported at different wavelengths.[8] In the present work, the concentration of Er^{3+} in both of the phases has been determined. Since no previous studies of Er^{3+}-doped $CaZrO_3$ or CaSZ were reported, we have grown Er^{3+}-doped single crystals of both phases found in the eutectic material and characterized them spectroscopically. We discuss the optical properties of the Er^{3+}-doped eutectic crystals on this basis.

II. EXPERIMENTAL DETAILS

Crystals of the eutectic composition (40 mol % CaO+60 mol % ZrO_2 nominal), calcia-stabilized zirconia (25 mol % CaO+75 mol % ZrO_2 nominal), and $CaZrO_3$, all three doped

with 0.5 mol % Er_2O_3 were grown from sintered ceramic precursors by the laser floating zone method using an annular focused beam of a CO_2 laser. Details of the crystal-growth method are given elsewhere.[6] Crystals with cylindrical symmetry 50 mm long and 2 mm in diameter were obtained.

Electron probe microanalysis (EPMA) was performed in the three materials to evaluate the Er concentration. The x-ray energy dispersive spectra were acquired with a Jeol 6400 scanning electron microscope (SEM) using a Link Analytical eXL system equipped with a Si(Li) solid-state detector (resolution at 5.9 keV: 137 eV). Calibrated spectra of the analyzed cations were taken previously to the registration of the x-ray spectra from the samples to quantify them as precisely as possible.

Optical absorption measurements in the 300–2600 nm range were carried out with a Hitachi U-3400 spectrophotometer. To increase their signal-to-noise ratio, short focal length glass quartz lenses were used to focus the light onto the small samples. Polarization spectra in the 350–900 nm region were obtained using unsupported dichroic polarizers. The single crystals were oriented using the back-reflection Laue method with x-rays from a Cu anticathode tube operating at 45 kV and 25 mA.

Photoluminescence spectra were obtained by exciting the samples with light, either from a 1000 W tungsten lamp passed through a SPEX double monochromator ($f=0.22$ m), or from a pulsed tunable dye laser (DyeScan from EG&G). Fluorescence was detected through a 0.5 m Jarrell-Ash monochromator with a Hamamatsu R-928 photomultiplier, and Si or Ge diode detectors for a visible and infrared ranges of the spectrum. The signal from the detectors was acquired with a Tektronix 2430 digital oscilloscope controlled by a personal computer. Lifetimes were measured by modulating the light either with a mechanical chopper for lamp excitation (long lifetimes) or with the pulsed laser (short lifetimes). Variable temperatures from room temperature (RT) down to 10 K were achieved using a closed-cycle cryorefrigerator with an accuracy of ± 1 K, and from RT up to 600 K using a homemade coaxial heater and sample holder with an accuracy of ± 3 K.

The luminescence optical bench formed 90° with the excitation bench, and the sample was placed with the growth axis perpendicular to the plane formed by these two directions.

III. COMPOSITION AND MICROSTRUCTURE OF THE SAMPLES

Three Er-doped materials have been used in this study: $CaZrO_3$, CaSZ single crystals, and ZrO_2-CaO eutectics. The refractive index of 2.15 for $CaZrO_3$ and 2.20 for CaSZ was estimated by the apparent thickness method using an optical microscope and white light.

$CaZrO_3$ has the orthorhombic *Pcmn* perovskite structure (space group D_{2h}^{16}),[9] and thus it is a biaxial crystal. The orthorhombic lattice parameters are $a=5.5912$, $b=8.0171$, and $c=5.7616$Å. It presents a phase transition to the cubic structure at about 1600 °C (Ref. 10) or even higher temperatures,[11] which causes the orthorhombic crystal to be twinned.[12] This has in fact been observed in our $CaZrO_3$ samples, both in the eutectic and single crystal. In the single crystal, however, macroscopic regions (several squared millimeters) keep the *b*-axis orientation constant, and not far from the growth axis, and only *a* and *c* axes are interchanged from twin to twin. This has been observed following the micro-Raman spectra, which is the subject of a forthcoming publication. This region will present macroscopically the same optical behavior as an axial crystal. CaSZ has the fluorite structure O_h^5 and is optically isotropic.

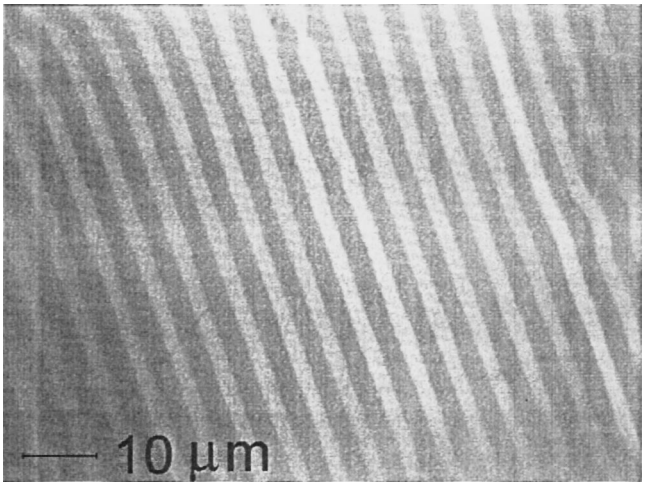

FIG. 1. Optical micrograph of the green Er^{3+} luminescence excited with $\lambda=514.5$ nm laser light.

The microstructure of the LFZ grown Er^{3+}-doped eutectic crystals is similar to the undoped ones.[6] It consists of ordered alternate $CaZrO_3$ and CaSZ lamellae. In Fig. 1 we present a microphotograph of a transverse section performed by illuminating a 1 mm thick sample with a 514.5 nm Ar^+ laser beam on the bottom surface. The picture shows the image observed on the upper surface using an orange filter to prevent the laser light from entering the camera. The green Er^{3+} luminescence is guided by the CaSZ lamellae (higher refractive index) as it has been recently proven elsewhere.[13]

EPMA was used to determine the Er concentration and Ca/Zr ratio in the phases of the eutectic crystal. Accordingly, within the eutectic sample the Er concentration in CaSZ (containing 24 mol % CaO) is three times higher than in $CaZrO_3$ ($3.3\pm0.3\times10^{20}$ cm^{-3} in CaSZ and $1.0\pm0.3\times10^{20}$ cm^{-3} in $CaZrO_3$).[14] This result is not surprising since CaSZ is a much more defective crystal than $CaZrO_3$ and forms a solid solution with Er_2O_3, keeping the fluorite structure. On the contrary, and according to the similarity of their ionic radii, Er^{3+} ions replace Ca^{2+} in $CaZrO_3$, hence generating cation vacancies as charge compensating defects.

Single crystals with a composition close to that of the phases of the eutectic were also produced and their chemical composition analyzed by EPMA. In this way we obtain Er^{3+}-doped CaSZ with an Er^{3+} concentration of $1.8\pm0.4\times10^{20}$ cm^{-3} and $CaZrO_3$ with $1.0\pm0.3\times10^{20}$ cm^{-3}.[14]

These numbers indicate that the distribution coefficient of Er^{3+} in both $CaZrO_3$ and CaSZ single crystals produced by LFZ is compatible with unity. However, the different kinetics of Er^{3+}incorporation into the two crystals produces a redistribution of the impurity into the eutectic between CaSZ and $CaZrO_3$ phases.

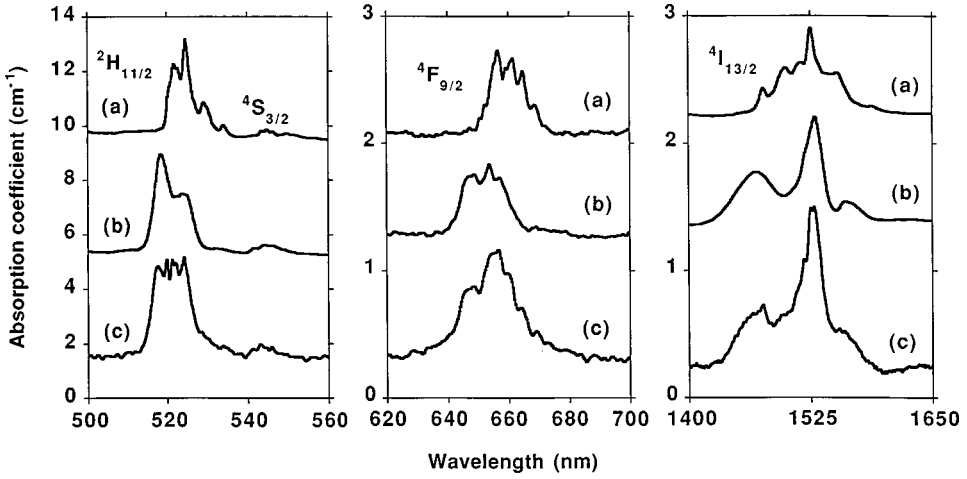

FIG. 2. Optical absorption bands of Er^{3+} from the ground state to the levels $^2H_{11/2}(^4S_{3/2})$, $^4F_{9/2}$, and $^4I_{13/2}$ measured at room temperature. (a) in $CaZrO_3$, (b) in CaSZ, and (c) in the eutectic crystal.

IV. EXPERIMENTAL RESULTS AND INTERPRETATION

The $f \rightarrow f$ spectra of trivalent lanthanide ions are mainly a consequence of forced electric dipole transitions due to $4f^N$ configuration mixing with other excited configurations of opposite parity. Such a mixing, and hence the oscillator strengths of the transitions, depends on the existence of odd-parity crystal-field potential terms (static contribution) and on the non totally symmetric lattice vibrations (dynamical contribution). Dynamic contribution is generally dominant for sites with inversion symmetry.

Intraconfigurational $f \rightarrow f$ transition probabilities can be calculated by the Judd-Ofelt (JO) theory[15,16] as a function of three parameters (intensity parameters) Ω_k $(k=2,4,6)$ that account for both static and dynamic configuration mixing. Usually, the intensity parameters describing a particular $4f$ system are found by fitting the theoretical values of the transition oscillator strengths predicted by JO theory to the experimental ones derived from optical absorption spectra. The maximum possible number of transitions are used to obtain a good fitting. Once the intensity parameters are found, it is easy to calculate radiative-transition probabilities, radiative lifetimes, and emission branching ratios, to be compared with experiments.

The JO theory is so commonly utilized that the reader may find information in many sources. As a reminder, this theory assumes that all the crystal-field Stark levels are equally populated. That is the reason why JO theory is generally used to analyze rare-earth ions room-temperature spectra.

A. Room temperature optical absorption of Er^{3+}

Figure 2 shows some optical absorption bands of Er^{3+}-doped eutectic [Fig. 2(c)], CaSZ:Er [Fig. 2(b)], and $CaZrO_3$ [Fig. 2(a)] measured at room temperature. The absorption bands correspond to f-f transitions from the $^4I_{15/2}$ Er^{3+} ground multiplet. No attention was given to the polarization of the incident light or the orientation of the $CaZrO_3$ crystal on these measurements. It can be seen that the optical absorption spectrum of Er^{3+}-doped ZrO_2-CaO consists of a weighted addition of CaSZ:Er^{3+} and $CaZrO_3$:Er^{3+} spectra, considering their Er^{3+} concentration and volume fractions in the eutectic sample ($v_{CaSZ}=0.4$, $v_{CaZrO_3}=0.6$) as determined by EPMA and SEM micrographs, respectively. Let us focus now on the absorption spectra of Er^{3+} ions in $CaZrO_3$ and CaSZ single crystals. The absorption wavelength (taken as the band centroid) and labeling of the excited levels are given in Tables I and II, respectively.

Er^{3+} enters the $CaZrO_3$ lattice in the Ca^{2+}sites (C_s point symmetry). Hence each of the J levels or the $4f^{11}$ Er^{3+} configuration splits into $(2J+1)/2$ Kramers doublets and no strict selection rule exist for the optical transitions. Polarized spectra are presented in Fig. 3 for the $^2H_{11/2}(^4S_{3/2})$ absorption, with the electric field either parallel or perpendicular to the b axis. Although some polarization of the bands is present, their integrated intensity remains constant within the experimental error of about 10%.

The oscillator strengths of the $J \rightarrow J'$ transitions f_{exp} have been obtained from the room-temperature area of the absorption bands using the expression

$$f(J,J') = \frac{mc^2}{\pi q^2 N} \int \frac{OD(\lambda)2.303}{L\lambda^2} d\lambda, \qquad (1)$$

TABLE I. Room-temperature absorption band positions (λ in nm), experimental (f_{exp}), and calculated (f_{calc}) oscillator strengths (in 10^{-8} units) of Er^{3+} in $CaZrO_3$.

Level	λ (nm)	f_{exp}	f_{calc}
$^4I_{13/2}$	1527	97.6+68.4[a]	144.8+68.4[a]
$^4I_{11/2}$	977	52.7	71.7
$^4I_{9/2}$	804		31.5
$^4F_{9/2}$	660	224.7	221.5
$^4S_{3/2}$	547	61.2	54.2
$^2H_{11/2}$	525	1079.4	1011.1
$^4F_{7/2}$	492	181.1	215.5
$^4F_{5/2}$, $^4F_{3/2}$	448		103
$^2H_{9/2}$	409	251.2	79.0
$^4G_{11/2}$	380	1746	1784

[a]Magnetic dipole contribution.

TABLE II. Room-temperature absorption band positions (λ in nm), experimental (f_{exp}), and calculated (f_{calc}) oscillator strengths (in 10^{-8} units) of Er^{3+} in CaSZ.

Level	λ (nm)	f_{exp}	f_{calc}
$^4I_{13/2}$	1507	61.1+70[a]	93.8+70[a]
$^4I_{11/2}$	970	34.8	47.7
$^4I_{9/2}$	792		22.6
$^4F_{9/2}$	651	154.3	151.2
$^4S_{3/2}$	545	42.8	33.9
$^2H_{11/2}$	521	743	777.0
$^4F_{7/2}$	488	114.8	139.3
$^4F_{5/2}$, $^4F_{3/2}$	446		64.7
$^2H_{9/2}$	408	167.6	50.2
$^4G_{11/2}$	380	1382	1362.3

[a]Magnetic dipole contribution.

where m and q are the electron mass and charge respectively, c is the light velocity in vacuum, $OD(\lambda)$ the optical density as a function of wavelength λ, and L the thickness of the sample. N is the number of absorbing ions per unit volume. All the magnitudes are to be evaluated in cgs units.

Owing to the absence of polarization in the band integrated intensity and since nonpolarized spectra allow better signal-to-noise ratio to be reached by focusing the light beam on the sample, the oscillator strengths have been determined from nonpolarized spectra. In Tables I and II we give the oscillator strengths.

From the experimental absorption oscillator strength values and the reduced matrix elements of the unit tensor operators $U^{(t)}$ ($t=2,4,6$) taken from Ref. 17, we have calculated the radiative-transition probabilities making use of the JO theory. The intensity parameters Ω_k ($k=2,4,6$) obtained from the fitting of the oscillator strengths by the standard procedure described elsewhere[7] are reported in Table III. The oscillator strengths, calculated using these values and the JO theory, and the root-mean-square deviation of the fittings are given in Tables I, II, and III, respectively. The latter are within the usual range for this kind of analysis. As indicated in the tables, some of the bands have not been included in the fitting because of high uncertainty in the evaluation of their intensity. For the $^4I_{15/2}\rightarrow{}^4I_{13/2}$ absorption around 1550 nm the nonzero magnetic dipole contribution to the oscillator strength has been taken from Ref. 18.

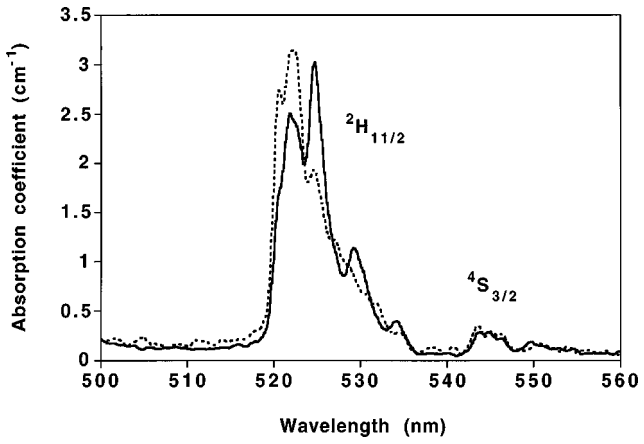

FIG. 3. Polarized absorption spectrum of Er^{3+} in $CaZrO_3$ to the level $^2H_{11/2}(^4S_{3/2})$, measured at room temperature. The solid line indicates the electric field parallel to the b axis and the dotted line indicates the electric field perpendicular to the b axis.

TABLE III. Judd-Ofelt parameters of Er^{3+} (in 10^{-20} cm^2) in several matrices, and root-mean-square deviations (rms) of f_{calc} given in Tables I and II.

Host	Ω_2	Ω_4	Ω_6	rms ($\times 10^7$)	Reference
$CaZrO_3$	4.13	1.00	0.87	8.9	This work
CaSZ	3.07	0.68	0.52	5.9	This work
50/50YSZ	2.92	0.78	0.57		Ref. 19

Higher Ω_k values are obtained for Er^{3+} in the orthorhombic $CaZrO_3$ crystal than in cubic CaSZ by a factor of about 1.5. This is a consequence of the absence of center of symmetry at the Er^{3+} site in this material, which allows for electric dipole $f\rightarrow f$ transitions. The cubic CaSZ matrix has a highly disordered fluorite-type lattice where ≈12% of the anionic sites are vacant. The distortion at the cation sites may also be responsible for the electric dipole allowed transitions. Here the Ω_k values are in close agreement with those obtained for Er^{3+} in yttria-stabilized zirconia containing 50 mol % Y_2O_3,[19] also given in Table III. Since this material presents 13% of oxygen vacancies, this similarity indicate that transition probabilities of optically active ions in zirconia matrices depend strongly on the oxygen sublattice disorder, whereas the stabilizing cation produces a negligible effect in those probabilities.

B. Luminescence at room temperature

Exciting the Er^{3+} absorption bands in the eutectic sample, an intense luminescence is observed. It corresponds to the green Er^{3+} luminescence (at 550 nm approximately) and red luminescence (around 660 nm) in the visible range. In addition, two luminescence bands are observed in the infrared (980 and 1530 nm).

In Fig. 4 we give the RT emission bands in the infrared, corresponding to the $^4I_{13/2}\rightarrow{}^4I_{15/2}$ and $^4I_{11/2}\rightarrow{}^4I_{15/2}$ transitions, excited in the $^2H_{11/2}$ or $^4F_{9/2}$ levels with broadband at wavelengths which give the maximum emission output. The luminescence bands corresponding to Er^{3+} in CaSZ and $CaZrO_3$ are also given in Fig. 4. Note that the CaSZ emission bands are broader than in $CaZrO_3$ as a consequence of the higher disorder in the lattice of the former. Note also that the eutectic $^4I_{13/2}\rightarrow{}^4I_{15/2}$ emission is dominated by the CaSZ contribution whereas in the $^4I_{11/2}\rightarrow{}^4I_{15/2}$ the main contribution comes from $CaZrO_3$. This interesting phenomenon has to do with the different excitation wavelengths, emission efficiencies, and branching ratios of the two components of the eutectic samples.

To elucidate that point we have measured the RT lifetimes of the four most intense emission bands in both CaSZ and $CaZrO_3$ single crystals to be compared with the ones calculated from JO theory. In Table IV we summarize these results. The observed decays are single exponential in $CaZrO_3$ where there is no evidence for more than one site for Er^{3+} in the matrix, that is the Ca^{2+} site. The decays in CaSZ have been measured with broadband excitation. They are not

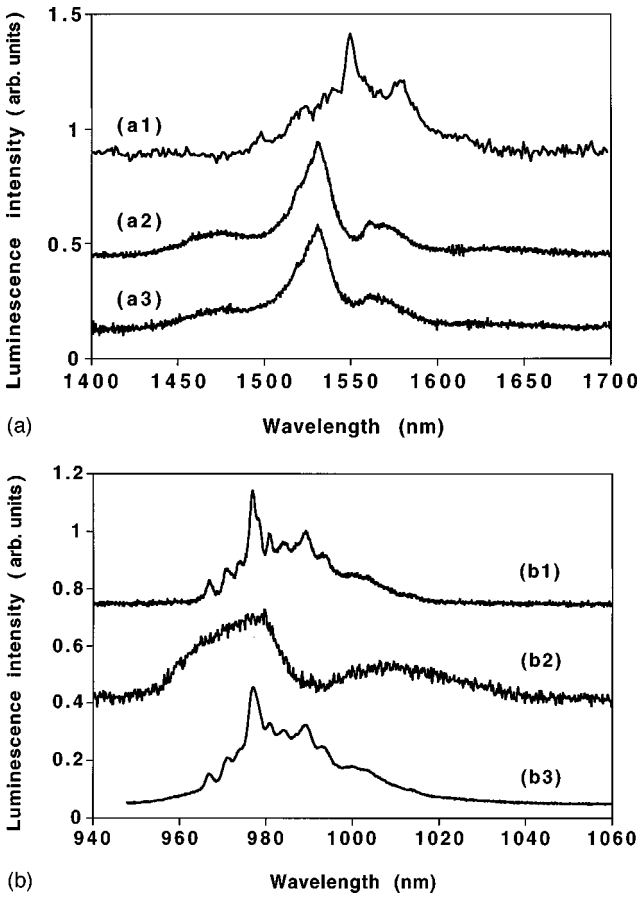

FIG. 4. Luminescence spectra or Er^{3+} in the three samples measured at room temperature. (a) Luminescence corresponding to the transition $^4I_{13/2} \rightarrow {}^4I_{15/2}$, with excitation bandpass of 14.4 nm into the green absorption band at (a1): 525.5 nm, (a2): 522.3 nm, and (a3): 522.3 nm. (b) Luminescence corresponding to the transition $^4I_{11/2} \rightarrow {}^4I_{15/2}$, with excitation bandpass of 14.4 nm into the red absorption band at (b1): 657.5 nm, (b2): 652.5 nm, and (b3): 657.5 nm. 1, 2, and 3 refer to the $CaZrO_3$, CaSZ, and eutectic samples, respectively. Excitation wavelengths have been chosen to give maximum luminescence intensity.

single exponential as it corresponds to a highly defective solid, and the lifetimes reported in Table IV correspond to half the time required to diminish the normalized intensity to $1/e^2$ (τ_2 in the following).

Several features are worth noting in Table IV. First of all, the radiative lifetimes of the $^4I_{13/2}$ level predicted by the Judd-Ofelt theory are shorter than the values found experimentally. As it can be seen in Tables I and II, the fitting fails to reproduce the $^4I_{15/2} \rightarrow {}^4I_{13/2}$ oscillator strength appropriately, the calculated transition probabilities being higher than the experimental ones (hence shorter calculated lifetimes). We have thus calculated directly the radiative lifetimes from the measured oscillator strengths, using the following relationship between oscillator strength for absorption and the radiative transition probability:

$$A(J \rightarrow J') = \frac{8(nq\pi\sigma)^2}{mc} \frac{2J'+1}{2J+1} f(J' \rightarrow J), \qquad (2)$$

where σ is the inverse of the wavelength of the transition in vacuum and n the refractive index of the material. Equation

TABLE IV. Room-temperature lifetimes, quantum efficiencies ($\eta = \tau_{exp}/\tau_{rad}$), and branching ratios [$\beta_{JJ'} = A(J,J')/\Sigma_{J'} A(J,J')$] for the observed luminescence bands.

$CaZrO_3$:Er

	Branching ratio $\rightarrow {}^4I_{13/2}$	Branching ratio $\rightarrow {}^4I_{15/2}$	τ_{rad}	τ_{exp}	η
$^4S_{3/2}(^2H_{11/2}) \rightarrow$	0.20	0.75	242 μs	195 μs	0.81
$^4F_{9/2} \rightarrow$	0.05	0.90	360 μs	39 μs	0.11
$^4I_{11/2} \rightarrow$	0.18	0.82	2.7 ms	2.4 ms	0.89
$^4I_{13/2} \rightarrow$		1	3.1 ms	4.5 ms	

CaSZ:Er

	Branching ratio $\rightarrow {}^4I_{13/2}$	Branching ratio $\rightarrow {}^4I_{15/2}$	τ_{rad}	τ_{exp}	η
$^4S_{3/2}(^2H_{11/2}) \rightarrow$	0.21	0.74	290 μs	47 μs	0.16
$^4F_{9/2} \rightarrow$	0.05	0.90	490 μs	5.2 μs	0.01
$^4I_{11/2} \rightarrow$	0.21	0.79	3.6 ms	0.9 ms	0.25
$^4I_{13/2} \rightarrow$		1	3.7 ms	6.3 ms	

(2) predicts 4.0 and 4.8 ms for the radiative lifetimes in $CaZrO_3$ and CaSZ, respectively. These values are still too low for CaSZ, even allowing for some uncertainty in the Er^{3+}concentration according to the chemical analysis data. The difference may arise from the different population of the Stark levels either for the ground-state multiplet, which has an effect in the absorption experiment, or for the $^4I_{13/2}$ multiplet, which perturbs the emission measurements, or both. On heating the sample, the radiative lifetimes decrease as it has been observed from 10 K to room temperature, where we can assume that no multiphonon relaxation is taking place because of the high-energy difference between $^4I_{13/2}$ and $^4I_{15/2}$ multiplets (more than 10 phonons are required to span the gap). The measured lifetimes of the $^4I_{13/2} \rightarrow {}^4I_{15/2}$ emission at 10 K are 5.1 and 7.3 ms in $CaZrO_3$ and CaSZ, respectively. It thus seems that there exist high-energy $^4I_{13/2}$ Stark levels with higher radiative-transition probabilities to the ground state ($^4I_{15/2}$), which are not equally populated even at RT. Note also that the quantum efficiencies ($\eta = \tau_{exp}/\tau_{rad}$) are higher for $CaZrO_3$ than for CaSZ, while branching ratios remain practically the same.

To end this section, we want to report on the emission lifetime measured in the eutectic sample. As it is clearly seen in Fig. 4, the luminescence bands contain a weighted mixture of CaSZ and $CaZrO_3$ luminescence bands, being the weights dependent on the pumping wavelength and the monitored luminescence. Decays are thus nonexponential unless the $CaZrO_3$ contribution dominates. The lifetimes for the levels $^4I_{13/2}$ in the CaSZ phase of the eutectic (6.2 ms) and that of $^4I_{11/2}$ in the $CaZrO_3$ phase (2.4 ms), are the same values as in the respective single crystals. Note especially that no lifetime shortening has been found in the CaSZ phase ($^4I_{13/2}$ level) that could have occurred if concentration quenching effects had started to contribute. Consequently, we can be sure that no concentration quenching effects take place in the $^4I_{13/2} \rightarrow {}^4I_{15/2}$ luminescence at this Er^{3+} concentration (3.3×10^{20} cm^{-3}). Due to the phase size (2 μm), no electronic energy transfer between Er^{3+} ions from phase to phase is expected.

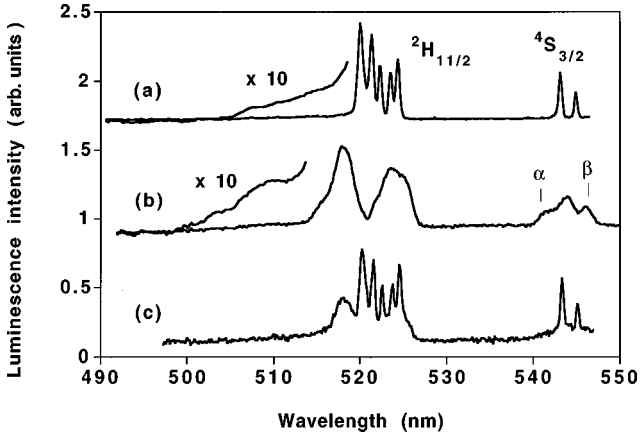

FIG. 5. Excitation spectra measured at 10 K on the three samples, monitoring the luminescence intensity at: (a) 550.3 nm for $CaZrO_3$, (b) 659.8 nm for CaSZ, and (c) 548.8 nm for the eutectic crystal. The low-intensity features observed at the high-energy side of the $^2H_{11/2}$ band correspond to vibronic sidebands.

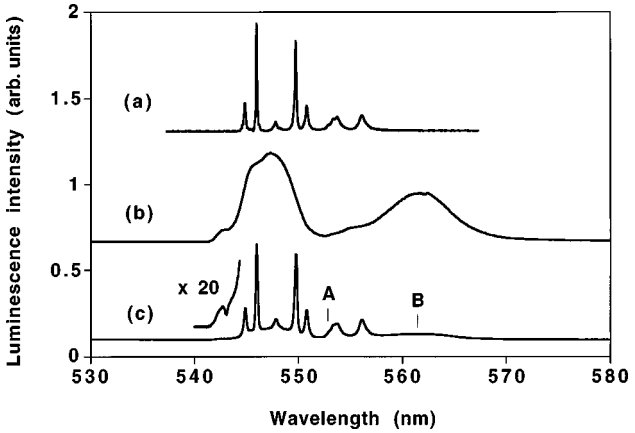

FIG. 6. Luminescence corresponding to the transition $^4S_{3/2} \rightarrow {}^4I_{15/2}$ measured at 10 K. Lamp excitation was made with wide bandpass at wavelengths: (a) 520 nm in $CaZrO_3$, (b) 377 nm in CaSZ, and (c) 519.3 nm in the eutectic sample.

C. Site resolved spectroscopy

To understand the Er^{3+} luminescence in the eutectic sample, site selective spectroscopy has to be made, and this is only feasible at low temperatures to prevent overlapping of the absorption or emission bands by thermal population of the excited Stark components of the ground or emitting multiplet, respectively. The smallness of the samples prevents us from measuring good absorption spectra, hence the study of the different sites will be based on luminescence and excitation experiments. From low-temperature emission spectra we can determine the levels of the ground multiplet and from low-temperature excitation spectra those of the excited levels.

In Fig. 5 we give the excitation spectra with resolution better than 0.36 nm, enough to position the Stark levels of the high-energy multiplets, of the $^4S_{3/2} \rightarrow {}^4I_{15/2}$ or $^4F_{9/2} \rightarrow {}^4I_{15/2}$ luminescence bands for the three samples detecting at 10 K with wide slit (3.2 or 1.6 nm bandpass). Bandwidths of $CaZrO_3$:Er levels are near to the better resolution of the experiment (11 cm^{-1} in the $^4S_{3/2}$ levels), while those of CaSZ:Er are of the order of 50 cm^{-1}. The eutectic excitation spectrum consists of a superposition of both CaSZ and $CaZrO_3$ bands.

In Fig. 6 we give the $^4S_{3/2} \rightarrow {}^4I_{15/2}$ emission bands measured at 10 K with narrow-band detection (better than 0.16 nm resolution) and 14.4 nm excitation bandpass. As in the case of excitation spectra, bandwidths are smaller for Er^{3+} in $CaZrO_3$ than in CaSZ, and the spectrum of the eutectic crystal consists of a superposition of the individual spectra.

Similar emission and excitation spectra have been performed for the different emission bands and the position of most of the multiplets determined. In Table V those positions for $CaZrO_3$:Er are summarized. Note that all the multiplets present a splitting lower than or equal to $J+\frac{1}{2}$, which is the maximum degeneracy possible in a C_s symmetry site. Accordingly, no more than one site of Er^{3+} in $CaZrO_3$ is present.

This is not the case in stabilized zirconia. Here different sites for Er^{3+} are expected,[7,20,21] which contribute to the large broadening of the bands. In fact, three maxima are found in the $^4I_{15/2} \rightarrow {}^4S_{3/2}$ absorption at wavelengths 542, 544, and 546 nm. The same three absorption maxima were present in yttria-stabilized zirconia with 5% oxygen vacancies (YSZ16),[7] and they were assigned to two different sites. The same assignment can be made here, one Er^{3+} site coordinated with 8 oxygens (CN8) with maximum at 542 nm (quasicubic symmetry), and the other with one oxygen vacancy in its first coordination shell (CN7) with maxima at 544 and 546 nm. As expected, the ratio CN7/CN8 sites is higher in the present case.

Site selection spectroscopy has also been performed in order to confirm this assumption. Site selective luminescence in the $^4S_{3/2}$ absorption band has been measured with the following results: Upon pulse excitation at 540.9 and 546.4 nm (marked α and β, respectively, in Fig. 5), decays are still nonexponential, the τ_2 values being 90 and 50 μs for α and β excitation, respectively. α and β excitations correspond to the two main sites present in the CaSZ structure, which can still be characterized by their first coordination shell according to their similarity with the YSZ16 spectra. Excitation on α gives a ground level splitting with levels at about 90, 230, and 590 cm^{-1} over the ground state, the splittings being slightly smaller than in YSZ16, and the site with β excitation gives ground-state splitting with levels at 30, 75, 260, and 520 cm^{-1}.

Site selective excitation has also been performed in the eutectic sample in the $^4I_{15/2} \rightarrow {}^4S_{3/2}$ band. Upon excitation in the $CaZrO_3$:Er^{3+} maxima of Fig. 5(c), luminescence spectra dominated by $CaZrO_3$:Er^{3+}spectra are obtained. They decay exponentially with 260 μs lifetime at 10 K, the same as in $CaZrO_3$ single crystals. Equivalently, upon excitation outside a $CaZrO_3$ peak, luminescence dominated by the corresponding selected site of Er^{3+} in CaSZ is obtained, similar to the CaSZ single crystal. No concentration quenching effects are observed for this luminescence.

V. DISCUSSION AND CONCLUSIONS

The microstructured optical material studied here contains a stack of $CaZrO_3$ and CaSZ alternate lamellae. The Er^{3+} active ion enters in the two phases with a different concen-

TABLE V. Stark levels of Er^{3+}-doped $CaZrO_3$.

Multiplet	Number of Stark levels	Energy (cm^{-1})
$^4I_{15/2}$	8	0, 40, 100, 163, 200, 282, 295, 373
$^4I_{13/2}$	7	6541, 6573, 6609, 6623, 6681, 6693
$^4I_{11/2}$	6	
$^4I_{9/2}$	5	
$^4F_{9/2}$	5	15 216, 15 246, 15 309, 15 340, 15 378
$^4S_{3/2}$	2	18 352, 18 413
$^2H_{11/2}$	6	19 069, 19 099, 19 142, 19 179, 19 205, 19 227
$^4F_{7/2}$	4	20 433, 20 492, 20 542, 20 585
$^4F_{5/2}$	3	22 139, 22 163, 22 193
$^4F_{3/2}$	2	22 472, 22 563
$^2H_{9/2}$	5	24 492 24 522, 24 618, 24 697
$^4G_{11/2}$	6	26 261, 26 344, 26 413, 26 455

tration, presumably due to the distinct solubility of the dopant in the respective crystals. As expected, the highly defective CaSZ crystal accommodates about three times more Er^{3+} from the melt than the nondefective $CaZrO_3$ crystal for the level of doping used in this experiment.

The Er^{3+} absorption and emission properties are also quite different for the two component crystals. For $CaZrO_3$:Er^{3+}, narrow and well-resolved absorption and emission bands are observed. As it corresponds to the larger oscillator strengths for absorption, the calculated radiative lifetimes are shorter than for CaSZ. In contrast with this, and with the exception of the lowest excited level emission $^4I_{13/2}$, the measured lifetimes are longer. This indicates that nonradiative-transition probabilities are larger in the defective CaSZ crystal than in $CaZrO_3$.This also produces a different distribution of the pumping energy among the luminescent levels, which explains, for example, the different relative intensities of the emission bands of the two component phases of the eutectic crystal, as shown in Fig. 4. So, we observe [see Fig. 4(a)] that when exciting in the efficient $^4I_{15/2}\rightarrow{}^2H_{11/2}$ hypersensitive absorption band, the luminescent $^4I_{13/2}$ level is better populated in CaSZ:Er^{3+} by the dominating nonradiative transitions from the excited levels than in the $CaZrO_3$:Er^{3+} where the nonradiative transitions are smaller. So, taking into account the main radiative and nonradiative deexcitation paths of the $^2H_{11/2}$ level to $^4I_{13/2}$ via the intermediate levels and using the numbers given in Table IV, 70% of the ions excited to the $^2H_{11/2}$ level in CaSZ:Er will contribute to the radiative transition $^4I_{13/2}\rightarrow{}^4I_{15/2}$, while only 21% will contribute in the $CaZrO_3$:Er^{3+} crystal. The emission from the $^4I_{11/2}$ excited in the $^4I_{15/2}\rightarrow{}^4F_{9/2}$ absorption band [Fig. 4(b)] presents the opposite behavior. There, the higher quantum efficiency of the luminescent $^4I_{11/2}$ level in $CaZrO_3$:Er^{3+}results in a more intense emission (of the ions excited to the $^4F_{9/2}$ level, 20% in CaSZ:Er^{3+} and 65% in $CaZrO_3$ will contribute to the radiative $^4I_{11/2}\rightarrow{}^4I_{15/2}$ luminescence, also from Table IV).

In order to find an explanation for the higher nonradiative-transition probabilities in CaSZ:Er^{3+} than in $CaZrO_3$:Er^{3+}, a single-phonon mode model of Riseberg and Moos has been used.[22] According to it, the temperature dependence of the nonradiative deexcitation probability (W_{NR}) is given by the expression

$$W_{NR}(T)=W_{NR}(0)\{\exp(\hbar\omega/kT)/[\exp(\hbar\omega/kT)-1]\}^p, \tag{3}$$

where $\hbar\omega$ is the phonon energy and $p=\Delta E/\hbar\omega$ is the number of phonons required to span the energy difference (ΔE) between the luminescent level and the electronic level immediately below it. ΔE can be obtained from absorption spectra. W_{NR} is calculated subtracting the radiative deexcitation probability ($1/\tau_{rad}$) from the measured one ($1/\tau_{exp}$), ($W_{NR}=1/\tau_{exp}-1/\tau_{rad}$). $W_{NR}(0)$ is the low-temperature multiphonon emission rate which is dependent on the energy gap and the electron-phonon coupling. This model applies to the case of low electron-phonon coupling and works satisfactorily for rare-earth ions.

Fitting of Eq. (3) to the nonradiative-transition probabilities of levels $^4S_{3/2}$ and $^4F_{9/2}$ in both CaSZ and $CaZrO_3$ crystals has been performed. The parameters obtained from the fits are summarized in Table VI. The phonon energies lie in the range 500–600 cm^{-1} in both cases, approaching the higher phonon energies which are Raman active,[6] (543 cm^{-1} in $CaZrO_3$ and 580 cm^{-1} in CaSZ). Vibronic sidebands are clearly seen in the excitation spectra measured at 10 K in some of the most intense transitions (to $^4F_{9/2}$, $^2H_{11/2}$, and $^4F_{7/2}$ in CaSZ or $^2H_{11/2}$, $^4F_{7/2}$, and $^4G_{11/2}$ in $CaZrO_3$), see for example, Fig. 5. They contain between 10 and 15% of the total excitation intensity and present a cutoff at about 530 cm^{-1} in $CaZrO_3$ and between 500 and 600 cm^{-1} in CaSZ, in accordance with the phonon energies of the multiphonon deexcitation fitting. Hence, it turns out that the energies of the phonons participating in the nonradiative deexcitation are of similar magnitude in both matrices, while the W_{NR} is still one order of magnitude higher in CaSZ than in $CaZrO_3$ for the same energy gap. The slightly lower phonon energies in

TABLE VI. Parameters obtained from the fitting to a Riseberg and Moos expression.

Host	Level	p	$\hbar\omega$ (cm^{-1})	$W_{NR}(0)$ (s^{-1})
$CaZrO_3$	$^4F_{9/2}$	5	530	1.65×10^4
	$^4S_{3/2}$	6	525	6.0×10^2
CaSZ	$^4F_{9/2}$	5	560	1.35×10^5
	$^4S_{3/2}$	6	510	9.5×10^3

the Raman spectrum for the latter cannot be the only reason for this difference in W_{NR}, and differences in the electron-phonon coupling must also be playing a role.

According to the neutron-diffraction data for $CaZrO_3$ given by Ref. 9, Ca^{2+} is coordinated to 8 oxygens with a mean distance of 2.57 Å whereas the next 4 oxygen ions are at distances in the 3.0–3.6 Å range. On the other hand, from site resolved spectroscopy we have proposed that Er^{3+} ions in the CaSZ fluorite structure are coordinated mainly with 8 or 7 oxygen ions. Assuming no distortions in this structure, the cation-oxygen distance is 2.23 Å (5.15 Å lattice parameter for CaSZ 24 mol % CaO). Furthermore, extended x-ray-absorption fine structure data[23] have shown that in Er_2O_3 stabilized ZrO_2 (5 mol % $ErO_{1.5}$), vacancies tend to be located in the vicinity of the host Zr^{4+} cation, thus producing a mean relaxation of oxygen ions outwards of the Er^{3+} ion and inwards in the Zr^{4+} vicinity. Assuming this also happens in our crystal in the vicinity of the Er^{3+} dopant, it forces a relaxation outward of the nearest neighboring oxygen ions to 2.32 Å, which is still a smaller distance than in $CaZrO_3$. Thus an increase in the overlapping of Er^{3+}-ligand wave functions in the former, and consequently a higher electron-phonon coupling is expected.

We turn now to a different effect found when we excite the eutectic sample with broad light beams and is a consequence of the multiphase character of the material. Due to the large inhomogeneous broadening in the CaSZ spectra, absorption and luminescence bands of the two phases overlap. Hence, upon excitation on a $CaZrO_3$:Er^{3+} absorption peak, some luminescence can be measured at *B* (Fig. 6). This luminescence has longer lifetimes than that corresponding to the CaSZ site, suggesting that either luminescence for $CaZrO_3$ is also present at 561.5 nm [*B* in Fig. 6(c)] or that some radiative transfer from $CaZrO_3$:Er^{3+} luminescence contributes to the excitation of CaSZ:Er^{3+}. The reverse effect of the latter (reabsorption of luminescence from CaSZ by $CaZrO_3$) has in fact been observed in the luminescence band of Fig. 6(c) with a dip at 543.1 nm, corresponding to the $CaZrO_3$:Er^{3+} absorption peak position.

To confirm this point, the excitation spectrum of the luminescence at *B* has been measured in the eutectic sample, and is shown in Fig. 7. The sharp peak at 544.9 nm (number 7) clearly corresponds to a $^4I_{15/2} \rightarrow {}^4S_{3/2}$ excitation of $CaZrO_3$:Er^{3+} luminescence. A careful examination of the $CaZrO_3$:Er^{3+} green luminescence spectrum [Fig. 6(a)] shows a low intensity tail at the long-wavelength side, probably due to vibronic transitions which overlap the CaSZ:Er^{3+} luminescence at *B*.

But much more intense are the dips detected in the $^4I_{15/2} \rightarrow {}^2H_{11/2}$ CaSZ:Er^{3+} excitation band. In the lower part of Fig. 7 we have marked the positions of the narrow $CaZrO_3$:Er^{3+} excitation peaks, numbered from 1 to 7. 1, 3, 4, and 5 coincide with the dips, while 7 clearly produces a peak. 2 and 6 might also produce a positive contribution to the excitation spectra.

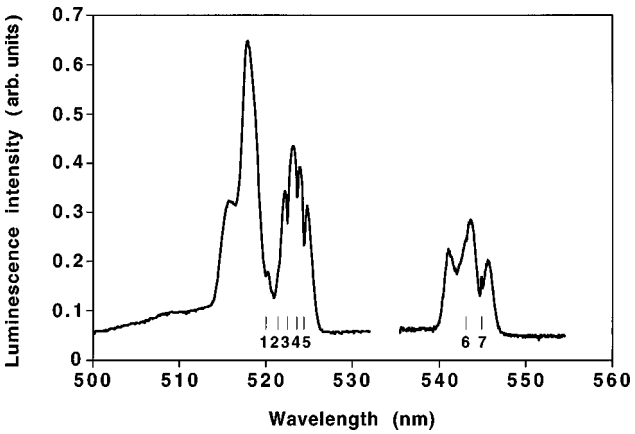

FIG. 7. Excitation spectrum of Er^{3+} into the eutectic crystal with detection wavelength at 561.5 nm [marked *B* in Fig. 6(c), which is a maximum of the CaSZ:Er^{3+} luminescence]. The position of the $CaZrO_3$:Er^{3+} excitation peaks are indicated with numbers 1 to 7.

The reason for the dips is obviously the absorption of incident light by the $CaZrO_3$ phase before arriving at the CaSZ phase. But, which is the reason for the peaks? From the absorption spectra in the single phase crystals, we have calculated the contribution from the two possible processes. Radiative transfer from $CaZrO_3$:Er^{3+} to CaSZ:Er^{3+} turns out to be too small to compensate for $CaZrO_3$:Er^{3+} absorption prior to CaSZ:Er^{3+} excitation, thus the underlying $CaZrO_3$:Er^{3+} luminescence at *B* is the reason for the peak at 544.9 nm (marked 7). Then, the spectrum in Fig. 7 can be understood as follows: If the $CaZrO_3$:Er^{3+} absorption coefficient is high, dips appear, whereas upon $CaZrO_3$:Er^{3+} absorption coefficient decreasing, those dips are compensated by $CaZrO_3$:Er^{3+} direct luminescence and finally peaks appear in the excitation spectrum. The relative weight of both effects depends very strongly on the geometry of the experiment and sample size.

In conclusion, we have prepared a structured composite material of two optical crystals with different refractive index. Three luminescent Er^{3+} sites have been identified, one in the $CaZrO_3$ phase and two in the CaSZ phase. The spectroscopic properties of these sites are quite different: narrow and well-resolved absorption and emission bands for the nondefective $CaZrO_3$ phase, and broad structureless bands for the highly defective CaSZ phase. The work opens new possibilities for light guiding and power amplification that are currently under study.

ACKNOWLEDGMENT

This work has been supported by the CICYT (Spain) under Contract No. MAT94-0225.

[1] A. Polman, D. C. Jacobson, D. J. Eaglesham, R. C. Kistler, and J. M. Poate, J. Appl. Phys. **70**, 3778 (1991).
[2] L. E. Bausá, G. Lifante, E. Daran, and P. L. Pernas, Appl. Phys. Lett. **68**, 3242 (1996).
[3] F. Schiller, B. Herreros, and G. Lifante, J. Opt. Soc. Am. A **14**, 425 (1997).
[4] E. Fogret, G. Fonteneau, J. Lucas, and R. Rimet, Opt. Mater. **5**, 79 (1996).
[5] W. J. Minford, R. C. Bradt, and V. S. Stubican, J. Am. Ceram. Soc. **62**, 154 (1979).
[6] J. I. Peña, R. I. Merino, G. F. de la Fuente, and V. M. Orera, Adv. Mater. **8**, 909 (1996).
[7] R. I. Merino, V. M. Orera, R. Cases, and M. A. Chamarro, J. Phys.: Condens. Matter **3**, 8491 (1991).
[8] V. I. Aleksandrov, M. A. Vishnyakova, V. P. Voitsitskii, E. E. Lomonova, M. A. Noginov, V. V. Osiko, V. A. Smirnov, A. F. Umyskov, and I. A. Shcherbakov, Sov. J. Quantum Electron. **19**, 1555 (1989).
[9] H. J. A. Koopkans, G. M. H. van de Velde, and P. J. Gellings, Acta Crystallogr., Sect. C. **39**, 1323 (1983).
[10] M. Foëx, J. P. Traverse, and J. Coutures, C. R. Acad. Sci. **264**, 1837 (1967).
[11] V. Stubican, in *Science and Technology of Zirconia III*, edited by S. Somiya, N. Yamamoto, and H. Yanagida (The American Ceramic Society, Westerville, OH, 1986), pp. 71–82.
[12] V. P. Dravid, C. M. Sung, M. R. Notis, and C. E. Lyman, Acta Crystallogr., Sect. B **45**, 218 (1989).
[13] V. M. Orera, J. A. Lázaro, J. A. Vallés, J. I. Peña, R. I. Merino, M. A. Rebolledo, Appl. Phys. Lett. (to be published).
[14] The numbers indicating the errors on the concentration values are the standard deviation from the fitting procedure.
[15] B. R. Judd, Phys. Rev. **127**, 750 (1962).
[16] G. S. Ofelt, J. Chem. Phys. **37**, 511 (1962).
[17] W. T. Carnall, H. Crosswhite, and H. M. Crosswhite, Argonne National Laboratory Report No. ANL-78-XX-95 (1978).
[18] W. T. Carnall, P. R. Fields, and K. Rajnak, J. Chem. Phys. **49**, 4412 (1968).
[19] E. Greenberg, G. Katz, R. Reisfeld, N. Spector, R. C. Marshall, B. Bendow, and R. N. Brown, J. Chem. Phys. **77**, 4797 (1982).
[20] H. Arashi, Phys. Status Solidi A **10**, 107 (1972).
[21] J. Dexpert-Ghys, M. Faucher, and P. Caro, J. Solid State Chem. **54**, 179 (1984).
[22] L. A. Riseberg and H. W. Moos, Phys. Rev. **174**, 429 (1968).
[23] M. Cole, C. R. A. Catlow, and J. P. Dragun, J. Phys. Chem. Solids **51**, 507 (1990).